IEEE Access
Multidisciplinary | Rapid Review | Open Access Journal

Received June 18, 2020, accepted June 28, 2020, date of publication July 9, 2020, date of current version July 22, 2020.

Digital Object Identifier 10.1109/ACCESS.2020.3008221

Optimized Scheme of Antenna Diversity for Radio Wave Coverage in Tunnel Environment

ZHENYU ZHAO[1,2], JUNHONG WANG[1,2], (Senior Member, IEEE), WEIBIN HOU[3], YUJIAN LI[1,2], (Member, IEEE), AND BO AI[4,5], (Senior Member, IEEE)

[1]Key Laboratory of All Optical Network and Advanced Telecommunication Network of MOE, Beijing Jiaotong University, Beijing 100044, China
[2]Institute of Lightwave Technology, Beijing Jiaotong University, Beijing 100044, China
[3]China Academy of Information and Communications Technology, Beijing 100191, China
[4]State Key Laboratory of Rail Traffic Control and Safety, Beijing Jiaotong University, Beijing 100044, China
[5]Beijing Engineering Research Center of High-speed Railway Broadband Mobile Communications, Beijing Jiaotong University, Beijing 100044, China

Corresponding author: Junhong Wang (wangjunh@bjtu.edu.cn)

This work was supported by the National Nature Science Foundation of China under Grant 61871025 and Grant 61331002.

ABSTRACT To suppress the deep fading of radio waves caused by the tunnel waveguide effect, this paper presents an optimized scheme for the spatial and polarization diversities of tunnel antennas. Through the correlation coefficient analysis of path loss curves obtained by antennas placed at different positions, the two antenna positions that generate path loss curves with the lowest correlation coefficient are found, and these two antennas are defined as a diversity antenna pair. Using this scheme, the spatial diversity properties of the transmitting antenna and receiving antenna, as well as the spatial-polarization combined diversity property of the transmitting antenna, are obtained. Furthermore, the impact of antenna polarization on the spatial diversity property is investigated. The performance of the proposed scheme for spatial and polarization diversities is evaluated in terms of the intensity and uniformity of the path loss. The simulation results illustrate that the proposed diversity optimization scheme can suppress the influence of the waveguide effect and achieve more uniform and flatter radio wave coverage in a tunnel environment.

INDEX TERMS Waveguide effect, spatial diversity, polarization diversity, correlation analysis, tunnel.

I. INTRODUCTION

Mobile communication has now entered the fifth-generation era and is applied to various scenarios where uniform radio coverage is desired. In tunnel environments, stable radio coverage is the basis for the safe operation of trains and good quality public communication. However, due to the waveguide effect, there are deep fading points of the received power distributed along a tunnel, which affect the wireless communication quality. Therefore, it is necessary to study the radio wave propagation property in tunnels and find ways to eliminate the deep fading points and achieve uniform radio wave coverage.

The radio wave coverage in the tunnel environment has been studied for a long time [1]–[3], and it can be modeled and predicted by measurements or by physics-based methods. Several measurement works on radio wave coverage in confined spaces have been published [4]–[6]. In [5], the radio wave transmission in the millimeter-wave band of 41 GHz for non-line-of-sight scenarios in a confined building corridor environment is measured. The channel characteristics, including the path loss model, root-mean-square delay spread, multipath statistics, small-scale fading characteristics, power delay profile, and power levels received from different antenna locations, are analyzed in detail. In [6], the extra loss caused by the tunnel curvature, frequency, polarization, and area of the cross section is analyzed by measurement. These measurement results can provide insights into the propagation characteristics of the studied channels, but it is time consuming and difficult to reveal the propagation mechanism. Among the physics-based methods, there are analytical approaches, such as waveguide theory [7], [8], and simulation techniques, such as the finite-difference time-domain (FDTD) [9], [10], vector parabolic equation (VPE) [11], [12], and ray tracing (RT) [13], [14] methods. Waveguide theory can be used to analyze the wave propagation characteristics in tunnels with regular cross sections effectively and accurately, but it is not

The associate editor coordinating the review of this manuscript and approving it for publication was Guido Valerio.

suitable for complex tunnel environments. The FDTD method was developed by solving Maxwell's equations through a numerical technique, has the advantages of simple iteration and high accuracy, and can directly give the time-domain solution of the field. However, this full-wave method requires a large number of computing resources, and its simulation efficiency is low. Therefore, some more effective and accurate deterministic models, such as the VPE and RT, have been applied to solve radio wave coverage in tunnels. The VPE method is highly efficient and suitable for large-scale environments, but it is effective only for the propagation of paraxial waves; hence, the calculation accuracy of wave propagation near the transmitting antenna is not high. Considering the accuracy and efficiency, this paper utilizes the ray tracing method based on geometrical optics to simulate tunnel environments with arbitrary geometries.

The radio wave coverage in tunnels is sensitive to the position of the antenna; thus, choosing an antenna position that results in uniform radio wave coverage in the tunnel environment is an important task. Many works have made attempts to achieve this goal. In [15], the optimum received power is achieved by arranging the discrete antenna positions in tunnels properly. In [16], a 2 × 2 MIMO array in the C-band is designed to increase the channel capacity. However, the deep fading points caused by the tunnel waveguide effect in these works are not suppressed. On the other hand, antenna diversity, which can overcome spatially selective fading and reduce the received power fluctuation in indoor, urban or suburban environments, has been studied by many researchers [17]–[19]. In [20], the effect of polarization diversity on channel capacity in arched tunnels is studied. In [21], it is found that a good quality signal can be achieved in almost the entire studied area by applying a large-scale diversity for antennas. However, these studies still have shortcomings in the suppression of deep fading caused by the waveguide effect in tunnel environments.

In this paper, an optimization scheme for spatial diversity and polarization diversity is proposed for suppressing the deep fading effect. The rest of this paper is organized as follows. Section II describes the simulation model of the tunnel and gives the mathematical formulation of the correlation coefficient. Section III presents the principle of correlation analysis between any two pairs of path loss curves obtained by changing the antenna position. According to the antenna pairs selected in Section III, spatial diversity for the transmitting and receiving antennas, as well as spatial-polarization combination diversity for the transmitting antennas, are achieved in Section IV. An analysis of the diversity scheme from the perspective of the transmission mode is presented in Section V. The conclusions are given in Section VI.

II. SIMULATION MODEL AND FORMULATION

Considering the accuracy and efficiency of numerical methods, an image-based ray tracing method is employed to model the radio wave propagation in tunnels. With this method, radio wave coverage as a function of the antenna parameters, such as location and polarization, can be studied.

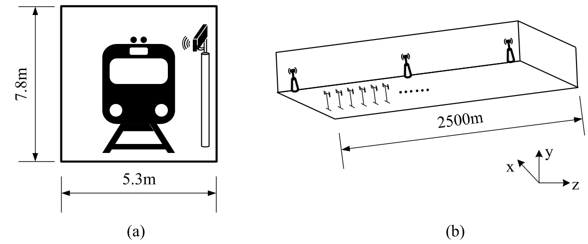

FIGURE 1. System model diagram of (a) the tunnel cross section and (b) the simplified communication system.

A. SYSTEM MODEL

As shown in Fig. 1 (a), a rectangular tunnel that is 7.8 m in width, 5.3 m in height and 2500 m in length is considered in this paper. The relative dielectric constant and conductivity of the tunnel walls are 5 and 0.01 S/m, respectively. The receiving antennas are mounted on the front panel of the train, and the transmitting antennas are mounted near the inner wall of the tunnel. When the train moves along the rail tracks, the received signal can be seen as the signals received by a series of receiving antennas placed along the route of the train, as shown in Fig. 1 (b). In this paper, the transmitting antenna is modeled by a Gaussian beam with a pencil pattern, and the receiving antenna is a dipole. Both the transmitting and receiving antennas work at a frequency of 900 MHz.

B. CORRELATION ANALYSIS MODEL

To compare the variation trends and correlation degree of the path loss curves obtained from antennas located at different positions, the Pearson correlation coefficient formula is used, which is given by

$$\rho_{X,Y} = \frac{\sum_1^N (X_i - \overline{X})(Y_i - \overline{Y})}{\sqrt{\sum_1^N (X_i - \overline{X})^2 \sum_1^N (Y_i - \overline{Y})^2}} \quad (1)$$

where X and Y are two discrete random variables, which represent the path losses obtained by two antennas working individually at different positions. N represents the number of discrete receiving points on each path loss curve. $\overline{X}$ and $\overline{Y}$ represent the average path loss of all discrete receiving points on each curve. In other words, when considering transmitting diversity, X is a discrete random variable composed of path loss values measured at discrete points along the receiving route when the transmitting antenna is installed at a certain position, and Y is another discrete random variable when the transmitting antenna is installed at another position. For receiving diversity, X is a discrete random variable composed of path loss values measured at discrete points by a receiving antenna located at a certain position on the moving object, and Y is another discrete random variable when the receiving antenna is located at another position on the moving object. A positive correlation coefficient means that the two path loss

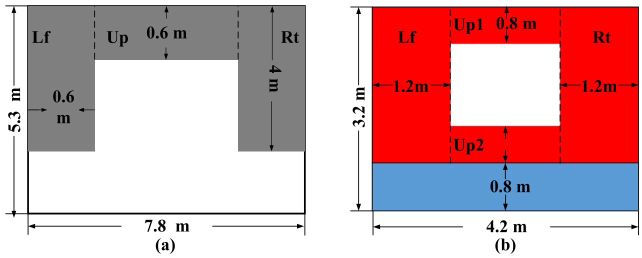

FIGURE 2. Position variation range of (a) the transmitting diversity antenna and (b) the receiving diversity antenna.

curves have the same variation trend. Conversely, a negative value means the opposite trend. A larger correlation coefficient indicates a stronger correlation.

III. CHANGE IN ANTENNA POSITION AND CORRELATION ANALYSIS

To ensure the accuracy of the simulation results, the numbers of reflection rays calculated in the horizontal and vertical directions are both set to 40. Moreover, to provide more data for the antenna location diversity reference, cases of hundreds of transmitting antenna and receiving antenna positions are simulated. The correlation analysis of any two path loss curves is carried out to find the diversity antenna pair locations with the lowest correlation coefficient.

Considering the practical installation requirements, a position change of the transmitting antenna will be restricted to the gray area, as shown in Fig. 2 (a). The receiving antenna is located at the front panel of the train, and the size of the simulated train model is based on that of a realistic train whose width and height are 4.2 m and 3.2 m, respectively. The position change range of the receiving antenna is set within the red area of Fig. 2 (b). When considering the position change of the transmitting antenna, the receiving antenna is fixed on the front panel of the train, which moves along the centerline of the tunnel; when changing the position of the receiving antenna, the transmitting antenna is fixed at the vertical central axis of the tunnel cross section on the entrance plane and 0.282 m away from the upper wall of the tunnel.

To analyze the spatial diversity and the spatial-polarization combined diversity properties, four polarization combinations of the transmitting and receiving antennas are considered. In each case, movement of the position of the diversity antenna in both the vertical and horizontal directions occurs in increments of 0.2 m. Therefore, for the entire area shown in Fig. 2(a), a total of 296 transmitting antenna positions are simulated for each polarization case when transmitting diversity, and a total of 200 receiving antenna positions are simulated for the entire area shown in Fig. 2(b) when receiving diversity.

For a transmitting antenna at each position in the area of Fig. 2 (a), diversity analysis is performed by comparing the correlation coefficients between the path loss curve of this transmitting antenna and the path loss curves of the transmitting antennas at all the other positions in the area of Fig. 2 (a). Similarly, for the receiving antenna at each position in the area of Fig. 2 (b), the diversity analysis is performed by comparing the correlation coefficients between the path loss curve of this receiving antenna and the path loss curves of the receiving antennas at all the other positions of Fig. 2 (b). Therefore, for each transmitting or receiving antenna at each position, a transmitting or receiving antenna with the lowest correlation coefficient can be found at another position. We call these two transmitting or receiving antennas the transmitting diversity antenna pair or receiving diversity antenna pair, and the number of diversity pairs is equal to the number of antenna positions.

IV. DIVERSITY RESULTS AND DISCUSSION

This section presents the diversity results of the four cases and analyzes the diversity effect. To determine the diversity effect more intuitively, in addition to directly observing the difference between the path loss curves obtained by a diversity antenna pair and a single antenna, this paper uses the median field intensity proposed in [22] and the system field strength flatness factor proposed in [23] to evaluate the slow and fast fading characteristics of the received power, respectively, for the cases of a single antenna and a diversity antenna pair. The isolation between two receiving or transmitting antennas of a transmitting diversity antenna pair or receiving diversity antenna pair and the channel capacity are provided.

The median field intensity can be used to represent the average strength of the received power, as expressed by

$$A_{Sa} = \frac{1}{x_0}\int_0^{x_0} A_S(x)dx \tag{2}$$

where x_0 is the length of the tunnel and A_s is the system median field intensity defined in [22]. The expressions of the system field strength flatness factor, which reflects the flatness characteristics of the received power, are given by

$$F_L(x) = \frac{\Delta_E(x)}{A_{Sa}} \tag{3}$$

$$F_{Lm} = \max\left[F_L(x)\right] \tag{4}$$

The isolation between antennas is required to be less than a specified threshold to avoid interference affecting the communication quality. The expressions of isolation are given by

$$L_v = 28 + 40\lg(\mathrm{k}/\lambda) \tag{5}$$

$$L_h = 22 + 20\lg(\mathrm{d}/\lambda) - (\mathrm{G_1} + \mathrm{G_2}) - (\mathrm{S_1} + \mathrm{S_2}) \tag{6}$$

$$L_s = (L_v - L_h)(\alpha/90) + L_h \tag{7}$$

where k and d are the distances of the two antennas in the vertical and horizontal directions, respectively. L_v and L_h are the vertical isolation and horizontal isolation between the two antennas, respectively. G is the antenna gain, and S is the sidelobe level of the antenna in the 90 degree direction. L_s is the isolation between two relatively inclined antennas, and α is the angle between the two antennas in the vertical plane. For the applied frequency in this paper, the threshold of isolation is 35 dB.

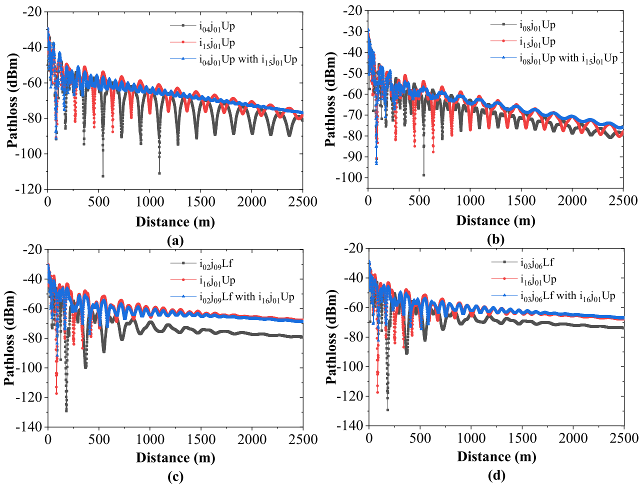

FIGURE 3. Simulated results of transmitting diversity: (a) pair A of the vertical polarization, (b) pair B of the vertical polarization, (c) pair C of the horizontal polarization, and (d) pair D of the horizontal polarization.

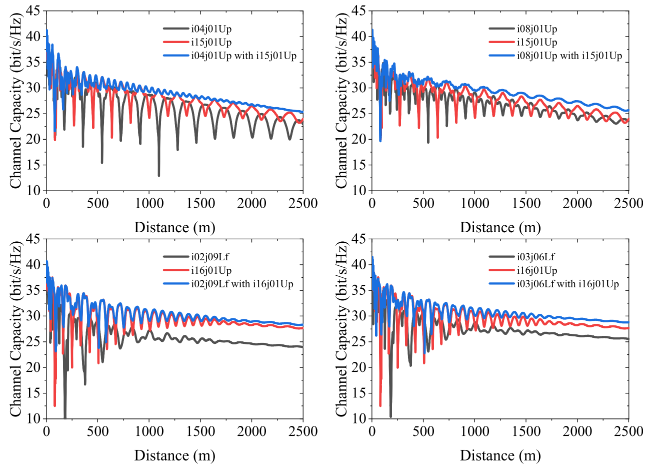

FIGURE 4. Channel capacity of transmitting diversity.

TABLE 1. Evaluation parameters of transmitting diversity.

	MEDIAN FIELD INTENSITY	FLATNESS FACTOR	MEDIAN FIELD INTENSITY OF NEAR FIELD	FLATNESS FACTOR OF NEAR FIELD	MEDIAN FIELD INTENSITY OF FAR FIELD	FLATNESS FACTOR OF FAR FIELD
$i_{04}j_{01}Up$ with $i_{15}j_{01}Up$	-59.9171	0.6095	-50.5256	0.6816	-62.3445	0.1899
$i_{04}j_{01}Up$	-67.9482	0.6143	-55.0517	0.6893	-71.2558	0.5348
$i_{15}j_{01}Up$	-67.9780	0.6154	-55.1693	0.5835	-71.2931	0.2905
$i_{08}j_{01}Up$ with $i_{15}j_{01}Up$	-58.6857	0.6009	-49.5847	0.6569	-61.0382	0.1761
$i_{08}j_{01}Up$	-65.4877	0.6092	-54.8564	0.5997	-68.2320	0.3999
$i_{15}j_{01}Up$	-67.9780	0.6154	-55.1693	0.5835	-71.2931	0.2905
$i_{02}j_{09}Lf$ with $i_{16}j_{01}Up$	-56.3231	0.5685	-49.0217	0.7411	-58.2283	0.1720
$i_{02}j_{09}Lf$	-69.7320	0.8061	-62.0713	1.0290	-71.7372	0.1981
$i_{16}j_{01}Up$	-69.7578	0.6360	-62.2035	0.8346	-71.7695	0.3270
$i_{03}j_{06}Lf$ with $i_{16}j_{01}Up$	-54.7783	0.5897	-47.6361	0.5966	-56.6402	0.2064
$i_{03}j_{06}Lf$	-64.6761	0.9491	-57.6355	1.1872	-66.5197	0.1878
$i_{16}j_{01}Up$	-64.7018	0.6270	-62.2035	0.8222	-71.7695	0.3270

The channel capacity per unit bandwidth can be estimated through the following expression:

$$C = \log\left(1 + \frac{P_r}{P_N}\right) \tag{8}$$

where P_r is the received power and P_N is the noise power.

A. TRANSMITTING DIVERSITY

As mentioned above, the transmitting diversity antenna pair is defined by two transmitting antennas Tx_{a_i} and $Tx_{a_ib_j}(j \neq i, i, j = 1, 2, 3 \ldots 296)$, where Tx_{a_i} is the transmitting antenna in a certain place in the gray area of Fig. 2(a) and $Tx_{a_ib_j}$ is the transmitting antenna in another place in the gray area of Fig. 2(a), the path loss curve of which has the lowest correlation coefficient with respect to that of Tx_{a_i}. According to this definition, a matching transmitting diversity antenna pair can be found for each transmitting antenna in Fig. 2(a). The influence of antenna polarization on the diversity property can also be obtained. Since too many antenna positions have been considered, for each polarization case, only two examples of the diversity effects between two antenna pairs in the area of Fig. 2(a) are given. For transmitting diversity in the vertical polarization, the results of the two diversity pairs (pair A and pair B) are shown in Fig. 3 (a) and (b), respectively, and for transmitting diversity in the horizontal polarization, the results of the two diversity pairs (pair C and pair D) are shown in Fig. 3 (c) and (d), respectively. The channel capacities for these four transmitting diversity pairs are shown in Fig. 4.

In Fig. 3, the black curve shows the path loss curve obtained from the single transmitting antenna Tx_{a_i}, the red line represents the path loss curve obtained from the single transmitting antenna $Tx_{a_ib_j}$, and the blue line represents the path loss curve obtained from the diversity array of both. In the legend of Fig. 3, i_mj_nK denotes that the transmitting antenna is located in the K region (Up or Lf, shown in Fig. 2) at positions m (steps) and n (steps). It can be seen that by this scheme of selecting the transmitting antenna diversity pair, a relatively stable and uniform receiving field can be realized in the tunnel environment, and the waveguide effect can be suppressed.

The evaluation parameters of the transmitting diversity antenna and single antenna are summarized in Table 1. For the vertical polarization, the transmitting diversity optimization region is mainly in the far region. It can be seen from Table 1 that compared with the single transmitting antenna, the median field intensity of the far field is increased by 13% after diversity is used, and the system field strength flatness factor is decreased by 60%. By contrast, for the horizontal polarized transmitting diversity, the optimized region is mainly in the near region. Compared with the single transmitting antenna, the median field intensity in the near region is increased by 21%, and the system field strength flatness factor is decreased by 48%.

The results of the isolation between the two transmitting antennas in each diversity combination are summarized in Table 4. The isolations of the four selected transmitting diversity cases all satisfy the requirements. In addition, from the data in Fig. 4, we can see that the channel capacity after diversity is improved in the far field.

B. RECEIVING DIVERSITY

Similarly, the receiving diversity antenna pair is defined by two receiving antennas Rx_{a_i} and $Rx_{a_ib_j}(j \neq i, i, j = 1, 2, 3 \ldots 200)$, where Rx_{a_i} is the receiving antenna in a

TABLE 2. Evaluation parameters of receiving diversity.

	MEDIAN FIELD INTENSITY	FLATNESS FACTOR	MEDIAN FIELD INTENSITY OF NEAR FIELD	FLATNESS FACTOR OF NEAR FIELD	MEDIAN FIELD INTENSITY OF FAR FIELD	FLATNESS FACTOR OF FAR FIELD
$i_{03}j_{01}Up$ with $i_{01}j_{01}Lf$	-64.5486	0.6339	-54.3126	0.5649	-67.1921	0.1602
$i_{03}j_{01}Up$	-69.9336	0.6578	-59.1489	0.5954	-72.7217	0.3860
$i_{01}j_{01}Lf$	-69.9663	0.5752	-59.2790	0.5451	-72.7626	0.2346
$i_{03}j_{04}Up$ with $i_{01}j_{01}Lf$	-65.1074	0.6546	-53.9392	0.5831	-67.9838	0.1736
$i_{03}j_{04}Up$	-71.5444	0.6996	-59.1778	0.6369	-74.7281	0.3031
$i_{01}j_{01}Lf$	-69.9663	0.5752	-59.3082	0.5451	-72.7626	0.2346
$i_{02}j_{02}Up$ with $i_{01}j_{01}Lf$	-59.7848	0.6314	-51.0262	0.5681	-62.0585	0.1370
$i_{02}j_{02}Up$	-64.4760	0.9636	-54.4225	0.8813	-67.0765	0.8875
$i_{01}j_{01}Lf$	-64.5052	0.5661	-54.5740	0.5800	-67.1130	0.4980
$i_{01}j_{13}Lf$ with $_{07}j_{01}Lf1$	-62.6690	0.6631	-52.6792	0.5992	-65,2504	0.1528
$i_{01}j_{13}Lf$	-73.6859	0.9964	-60.3580	1.4372	-77.1069	0.3294
$i_{07}j_{01}Lf$	-73.7149	0.6018	-60.4983	0.5149	-77.1431	0.3047

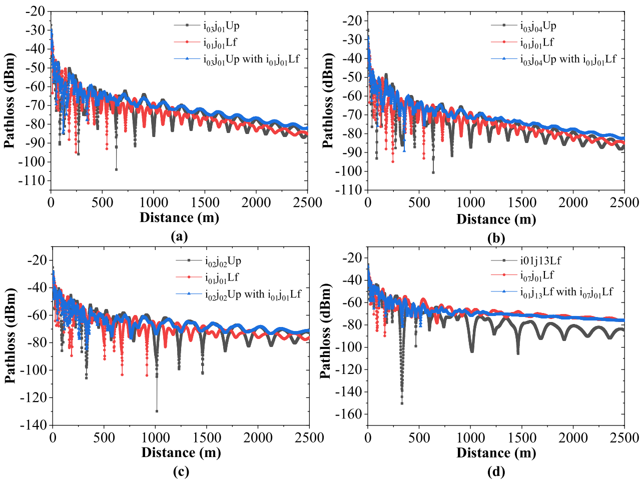

FIGURE 5. Simulated results of receiving diversity: (a) pair A of the vertical polarization, (b) pair B of the vertical polarization, (c) pair C of the horizontal polarization, and (d) pair D of the horizontal polarization.

certain place in the red area of Fig. 2(b) and $Rx_{a_ib_j}$ is the receiving antenna in another place in the red area of Fig. 2(b), the path loss curve of which has the lowest correlation coefficient with respect to that of Rx_{a_i}. According to this definition, a matching receiving diversity antenna pair can be found for each receiving antenna position in Fig. 2(b). The influence of antenna polarization on the diversity property is also obtained. For each polarization case, only two examples of the diversity effects between two antenna pairs in the area of Fig. 2(b) are shown in Fig. 5, and the evaluation parameters of the cases are listed in Table 2. The channel capacities for these four receiving diversity pairs are shown in Fig. 6.

It can be observed from Fig. 5 that the receiving antenna diversity can also give flat field distributions in the tunnel environment. Compared with the single receiving antenna, the receiving diversity antenna pairs in the vertical polarization can give a better distribution in the near region and remove the deep fading, the median field intensity in the near region increases by 11% and the system field strength flatness factor decreases by 5%. Similarly, the receiving diversity in the horizontal polarization can give a flatter field distribution in the far region with a weak waveguide effect. Moreover, from the evaluation parameters shown in Table 2, the receiving diversity for the horizontal polarization can reduce the system field strength flatness factor by approximately 50%.

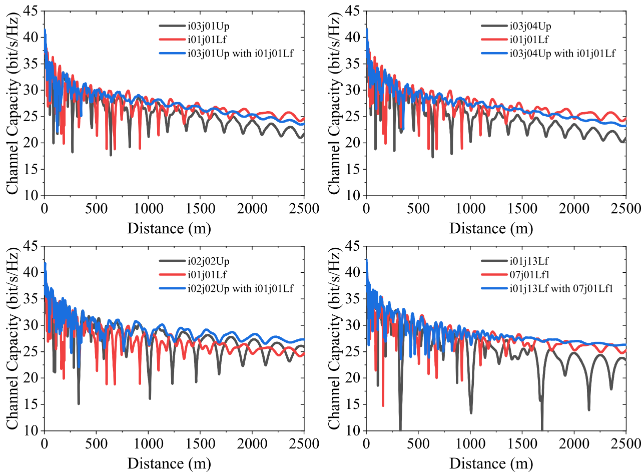

FIGURE 6. Channel capacity of receiving diversity.

TABLE 3. Evaluation parameters of combined diversity.

	MEDIAN FIELD INTENSITY	FLATNESS FACTOR	MEDIAN FIELD INTENSITY OF NEAR FIELD	FLATNESS FACTOR OF NEAR FIELD	MEDIAN FIELD INTENSITY OF FAR FIELD	FLATNESS FACTOR OF FAR FIELD
$i_{16}j_{01}$_Up_vp with $i_{03}j_{13}$_Lf_hp	-58.7979	0.6007	-50.7791	0.6645	-60.8837	0.1917
$i_{16}j_{01}$_Up_vp	-63.3449	0.5846	-52.4662	0.5270	-66.1489	0.2634
$i_{03}j_{13}$_Lf_hp	-63.3737	0.8677	-52.5925	1.2505	-66.1848	0.1166
$i_{03}j_{02}$_Lf_vp with $i_{26}j_{02}$_Up_hp	-51.6579	0.5542	-46.1777	0.5013	-53.1011	0.1235
$i_{03}j_{02}$_Lf_vp	-72.0362	0.6001	-58.0640	0.7386	-75.6159	0.4133
$i_{26}j_{02}$_Up_hp	-72.0594	0.6622	-58.1719	0.5816	-75.6448	0.3849

From Table 4, we can see that the isolations of the four selected receiving diversity schemes all satisfy the requirements. From the data in Fig. 6, we can see that the channel capacity after diversity is not degraded.

C. SPATIAL-POLARIZATION COMBINED DIVERSITY

A spatial-polarization combined diversity array is composed of a pair of horizontally polarized transmit-receive antennas and a pair of vertically polarized transmit-receive antennas. The polarization diversity is defined by the different polarization states between the two antenna pairs. The spatial diversity here is defined by the two positions of the transmitting antennas, which is similar to the above transmitting diversity case but with the polarization of the two transmitting antennas being in the orthogonal state. The positions of the receiving antennas in the two pairs here are fixed in the center of the locomotive. Correlation analysis of the path loss curves between the pairs of vertically and horizontally polarized transmit-receive antennas is carried out, and the two pairs of orthogonal polarized transmit and receive antennas with the lowest correlation coefficient are defined as spatial-polarization combined diversity antenna pairs. Parts of the results of the spatial-polarization combined diversity are shown in Fig. 7, and the evaluation parameters of the path loss are summarized in Table 3. The channel capacities of the two spatial-polarization combined diversity pairs are shown in Fig. 8.

It can be seen from Fig. 7 that the spatial-polarization combined diversity can suppress the deep fading phenomenon,

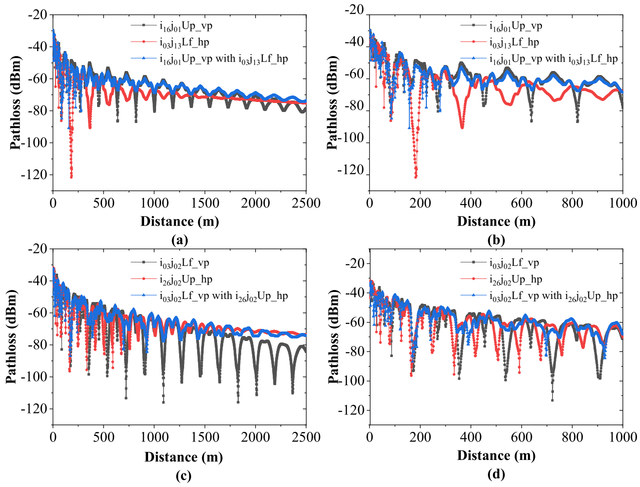

FIGURE 7. Simulated results of spatial-polarization combined diversity: (a) pair A, (b) local enlarged drawing of pair A, (c) pair B, and (d) local enlarged drawing of pair B.

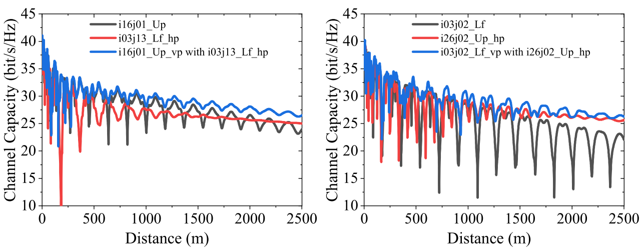

FIGURE 8. Channel capacity of spatial-polarization combined diversity.

TABLE 4. Isolation between antennas.

	MEDIAN FIELD INTENSITY
$i_{04}j_{01}Up$ with $i_{15}j_{01}Up$	57.0121
$i_{08}j_{01}Up$ with $i_{15}j_{01}Up$	53.0862
$i_{02}j_{09}Lf$ with $i_{16}j_{01}Up$	58.4746
$i_{03}j_{06}Lf$ with $i_{16}j_{01}Up$	61.7063
$i_{03}j_{01}Up$ with $i_{01}j_{01}Lf$	51.0204
$i_{03}j_{04}Up$ with $i_{03}j_{01}Lf$	55.8047
$i_{02}j_{02}Up$ with $i_{01}j_{01}Lf$	52.7735
$i_{01}j_{13}Lf$ with $_{07}j_{01}Lf1$	54.8601
$i_{16}j_{01}$_Up_vp with $i_{03}j_{13}$_Lf_hp	59.5513
$i_{03}j_{02}$_Lf_vp with $i_{26}j_{02}$_Up_hp	67.0803

especially in the near region, where some deep fading points are eliminated. From the evaluation parameters in Table 3, we can see that the median field intensity and the system field strength flatness factor are also improved.

From Table 4, we can see that the isolations of the four selected combined diversity schemes all meet the requirements. From the data in Fig. 8, we can see that the channel capacity after the implementation of diversity is improved in the far field.

V. MODE ANALYSIS

To understand the principle of the proposed diversity scheme, we analyze the proposed diversity scheme from the perspective of the transmission mode. It is quite accurate to calculate the mode phase and attenuation constant of the low-order modes by solving the mode equation as long as the diameter

TABLE 5. The sum of $E_{0,m,n}$ for combined diversity.

	$E_{0,0,1}$	$E_{0,0,2}$	$E_{0,0,3}$	SUM OF THE THREE MODES
$i_{04}j_{01}Up$ with $i_{15}j_{01}Up$	0.1003	0.0040	0.1000	0.2043
$i_{04}j_{01}Up$	0.0099	0.0039	0.0099	0.0239
$i_{15}j_{01}Up$	0.0048	0.0019	0.0048	0.0115
$i_{08}j_{01}Up$ with $i_{15}j_{01}Up$	0.2028	0.0807	0.2026	0.4861
$i_{08}j_{01}Up$	0.0162	0.0643	0.0161	0.0967
$i_{15}j_{01}Up$	0.0048	0.0190	0.0048	0.0286
$i_{02}j_{09}Lf$ with $i_{16}j_{01}Up$	0.1731	0.0049	0.1730	0.3510
$i_{02}j_{09}Lf$	0.0021	0.0083	0.0021	0.0125
$i_{16}j_{01}Up$	0.1541	0.0061	0.1539	0.3141
$i_{03}j_{06}Lf$ with $i_{16}j_{01}Up$	0.1353	0.0054	0.1351	0.2758
$i_{03}j_{06}Lf$	0.0095	0.0038	0.0095	0.0228
$i_{16}j_{01}Up$	0.0154	0.0061	0.0154	0.0369

of the tunnel is large enough relative to the applied wavelength [7]. The natural modes supported by a rectangular tunnel surrounded by a lossy medium are hybrid modes of the index mn, with all three components of the electric and magnetic field present. Any electric-field component $E(x, y, z)$ can be expressed as a modal summation [24]

$$\overrightarrow{\mathrm{E}}(\mathrm{x},\mathrm{y},\mathrm{z}) = \sum_{\mathrm{m}}\sum_{\mathrm{n}} \mathrm{E}_{0,\mathrm{m},\mathrm{n}} \cdot \overrightarrow{\mathrm{e}}_{\mathrm{m},\mathrm{n}}(\mathrm{x},\mathrm{y}) \cdot e^{-\beta_{\mathrm{m,n}}\mathrm{z}} \quad (9)$$

where $E_{0,m,n}$ is the complex amplitude of the mn mode, $\overrightarrow{e_{mn}}$ is the modal eigenfunction, $\beta_{mn} = k_{mn} + \alpha_{mn}$ is the complex propagation constant, and k_{mn} and α_{mn} are the propagation and attenuation constants of the mn mode, respectively.

From the analysis in reference [25], we know that the source affects the field of each order mode along the tunnel by affecting $E_{0,m,n}$ in formula (9). The values of $E_{0,m,n}$ can be immediately estimated through the following expression:

$$\mathrm{E}_{0,\mathrm{m},\mathrm{n}} = \frac{\int_{\mathrm{S}} \left(\overrightarrow{\mathrm{E}}_{\mathrm{REF}} \times \overrightarrow{\mathrm{h}}^{*}_{\mathrm{m,n}}\right) \cdot \widehat{\mathrm{i}}_{\mathrm{z}} \mathrm{dS}}{\int_{\mathrm{S}} \left(\overrightarrow{\mathrm{e}}_{\mathrm{m,n}} \times \overrightarrow{\mathrm{h}}^{*}_{\mathrm{m,n}}\right) \cdot \widehat{\mathrm{i}}_{\mathrm{z}} \mathrm{dS}} \quad (10)$$

with S being the transversal tunnel section. $\vec{E}_{REF}$ is the electric field over the transversal reference section $z = z_{REF}$, and $\vec{h}_{m,n} \approx h^{y}_{m,n} \cdot \hat{i}_y = \frac{e^{x}_{m,n}}{\eta_0} \cdot \hat{i}_y$, with $\eta_0 = 120\pi\,\Omega$. For the tunnel in this paper, we calculated that the modes that dominate the far field of the simulated tunnel are TE_{01}, TE_{02}, and TE_{03}. Therefore, we calculated the sum of $E_{0,m,n}$ for the three main modes under the four transmitting diversity combinations mentioned in Section IV of this paper and compared it with the sum obtained when the single transmitting antenna is used. The values are summarized in Table 5.

It can be seen from the calculation results that the sum of the three main modes under the diversity result is larger than the sum of the main modes when the single antenna is used. This result means that the field of the three main modes accounts for a larger proportion in the total field, thus making the superimposed electric field more uniform.

VI. CONCLUSIONS

In this paper, an optimized scheme for spatial and polarization diversity antennas in a tunnel environment is proposed.

By finding the smallest correlation coefficient between path loss curves given by antennas at different positions, the diversity antenna pairs with the smallest correlation coefficient can be found. The diversity scheme proposed in this paper can reduce the influence of the waveguide effect significantly and result in more uniform and flatter radio wave coverage in the tunnel environment. Moreover, regarding the channel capacity, the peak throughput under a 100 M bandwidth can reach 1 G/s, and it steadily attenuates to 100 M/s at the tunnel exit. By combining polarization with diversity, the field distribution can be further improved. It is shown that an antenna closer to the center of the tunnel cross section is more likely to give a weak correlation, which becomes even weaker when the distance between the two antennas increases. This result means that a better diversity effect can be realized by properly increasing the distance between the two antennas and that the deep fading phenomenon caused by the waveguide effect can be further suppressed.

REFERENCES

[1] C. Briso-Rodríguez, P. Fratilescu, and Y. Xu, "Path loss modeling for train-to-train communications in subway tunnels at 900/2400 MHz," *IEEE Antennas Wireless Propag. Lett.*, vol. 18, no. 6, pp. 1164–1168, Jun. 2019.

[2] M. Ghaddar, I. Ben Mabrouk, M. Nedil, K. Hettak, and L. Talbi, "Deterministic modeling of 5G millimeter-wave communication in an underground mine tunnel," *IEEE Access*, vol. 7, pp. 116519–116528, 2019.

[3] H. Jiang, Z. Chen, J. Zhou, J. Dang, and L. Wu, "A general 3D non-stationary wideband twin-cluster channel model for 5G V2 V tunnel communication environments," *IEEE Access*, vol. 7, pp. 137744–137751, 2019.

[4] T. Zhou, H. Li, R. Sun, Y. Wang, L. Liu, and C. Tao, "Simulation and analysis of propagation characteristics for tunnel train-ground communications at 1.4 and 40 GHz," *IEEE Access*, vol. 7, pp. 105123–105131, 2019.

[5] G. Yue, D. Yu, H. Qiu, K. Guan, L. Yang, and Q. Lv, "Measurements and ray tracing simulations for non-line-of-sight millimeter-wave channels in a confined corridor environment," *IEEE Access*, vol. 7, pp. 85066–85081, 2019.

[6] D. P. He, B. Ai, K. Guan, Z. Zhong, B. Hui, J. Kim, H. Chung, and I. Kim, "Channel measurement, simulation, and analysis for high-speed railway communications in 5G millimeter-wave band," *IEEE Trans. Intell. Transp. Syst.*, vol. 19, no. 10, pp. 3144–3158, Oct. 2018.

[7] D. Dudley, M. Lienard, S. Mahmoud, and P. Degauque, "Wireless propagation in tunnels," *IEEE Antennas Propag. Mag.*, vol. 49, no. 2, pp. 11–26, Apr. 2007.

[8] X. Zhang and C. D. Sarris, "Vector parabolic equation-based derivation of rectangular waveguide surrogate models of arched tunnels," *IEEE Trans. Antennas Propag.*, vol. 66, no. 3, pp. 1392–1403, Mar. 2018.

[9] D. Li, J. Wang, G. Tian, J. Zhou, and X. Lv, "An efficient algorithm based on the equivalence principle and FDTD for wave propagation prediction in tunnels," in *Proc. Int. Appl. Comput. Electromagn. Soc. Symp.-China (ACES)*, Jul. 2018, pp. 1–2.

[10] M. M. Rana and A. S. Mohan, "Segmented-locally-one-dimensional-FDTD method for EM propagation inside large complex tunnel environments," *IEEE Trans. Magn.*, vol. 48, no. 2, pp. 223–226, Feb. 2012.

[11] X. Zhang and C. D. Sarris, "Statistical modeling of electromagnetic wave propagation in tunnels with rough walls using the vector parabolic equation method," *IEEE Trans. Antennas Propag.*, vol. 67, no. 4, pp. 2645–2654, Apr. 2019.

[12] X. Zhang, N. Sood, J. K. Siu, and C. D. Sarris, "A hybrid ray-tracing/vector parabolic equation method for propagation modeling in train communication channels," *IEEE Trans. Antennas Propag.*, vol. 64, no. 5, pp. 1840–1849, May 2016.

[13] D. Didascalou, T. M. Schafer, F. Weinmann, and W. Wiesbeck, "Ray-density normalization for ray-optical wave propagation modeling in arbitrarily shaped tunnels," *IEEE Trans. Antennas Propag.*, vol. 48, no. 9, pp. 1316–1325, 2000.

[14] N. Sood and C. D. Sarris, "Enabling accurate propagation modeling of complex tunnel geometries with ray-tracing," in *Proc. IEEE Int. Symp. Antennas Propag. USNC/URSI Nat. Radio Sci. Meeting*, Jul. 2017, pp. 1827–1828.

[15] X. Zhang, A. Ludwig, N. Sood, and C. D. Sarris, "Physics-based optimization of access point placement for train communication systems," *IEEE Trans. Intell. Transp. Syst.*, vol. 19, no. 9, pp. 3028–3038, Sep. 2018.

[16] J. A. Valdesueiro, B. Izquierdo, and J. Romeu, "On 2×2 MIMO observable capacity in subway tunnels at C-band: An experimental approach," *IEEE Antennas Wireless Propag. Lett.*, vol. 9, pp. 1099–1102, 2010.

[17] A. P. Sohrab, P. Karadimas, and Y. Huang, "Diversity antenna for vehicular communications in microwave and mm-wave bands," in *Proc. IEEE-APS Topical Conf. Antennas Propag. Wireless Commun. (APWC)*, Sep. 2019, pp. 109–111.

[18] M. J. Ben-Constenla, M. Arias, A. Garcia-Pino, and O. Rubinos, "Compact diversity antenna for DCS-UMTS indoor environments," in *Proc. 2nd Eur. Conf. Antennas Propag. (EuCAP)*, Nov. 2007, pp. 1–4.

[19] P. Fan, X. Cui, and M. Lu, "Space and frequency diversity characterization of mobile GNSS receivers in multipath fading channels," *Tsinghua Sci. Technol.*, vol. 25, no. 2, pp. 294–301, Apr. 2020.

[20] W. J. Liao, C. H. Chuang, and B. Y. Dai, "Field test results and analysis of a semi-automatic effective diversity gain measurement system for MIMO and diversity antennas," in *Proc. Int. Symp. Antennas Propag. (ISAP)*, Oct. 2016, pp. 146–147.

[21] C. Rizzo, J. L. Villarroel, and D. Tardioli, "Spatial diversity based coverage map building in complex tunnel environments," in *Proc. Int. Conf. Wireless Commun. Underground Confined Areas*, Aug. 2012, pp. 1–7.

[22] Z. Zhao, W. Hou, and J. Wang, "Effect of antenna location and polarization on radio wave propagation in tunnel," in *Proc. Int. Conf. Microw. Millim. Wave Technol. (ICMMT)*, May 2019, pp. 1–3.

[23] Z. Zhao and J. Wang, "Effect of antenna location on uniformity of radio wave coverage in rectangular tunnels with different cross section sizes," in *Proc. Int. Symp. Antenna Propag. (ISAP)*, Oct. 2019, pp. 1–3.

[24] S. Loyka, "Multichannel capacities of waveguide and cavity channels," *IEEE Trans. Veh. Technol.*, vol. 54, no. 3, pp. 863–872, May 2005.

[25] K. D. Laakmann and W. H. Steier, "Waveguides: Characteristic modes of hollow rectangular dielectric waveguides," *Appl. Opt.*, vol. 15, no. 5, pp. 1334–1340, May 1976.

ZHENYU ZHAO was born in Shandong, China, in 1994. She received the B.E. degree from the School of Mechanical and Information Engineering, Shandong University, China, in 2016. She is currently pursuing the Ph.D. degree with the Institute of Lightwave Technology, Beijing Jiaotong University.

Her research interests include computational electromagnetics and radio wave coverage.

JUNHONG WANG (Senior Member, IEEE) was born in Jiangsu, China, in 1965. He received the B.S. and M.S. degrees in electrical engineering from the University of Electronic Science and Technology of China, Chengdu, China, in 1988 and 1991, respectively, and the Ph.D. degree in electrical engineering from Southwest Jiaotong University, Chengdu, in 1994. He joined with the Department of Electrical Engineering, Beijing Jiaotong University, Beijing, China, as a Faculty Member, in 1995, where he was a Professor, in 1999. From January 1999 to June 2000, he was a Research Associate with the Department of Electric Engineering, City University of Hong Kong, Hong Kong. From July 2002 to July 2003, he was a Research Scientist with Temasek Laboratories, National University of Singapore, Singapore. He is currently with the Key Laboratory of all Optical Network and Advanced Telecommunication Network, Ministry of Education of China, Beijing Jiaotong Univeristy. He is also with the Institute of Lightwave Technology, Beijing Jiaotong University. His research interests include numerical methods, antennas, scattering, and leaky wave structures.

WEIBIN HOU was born in Hebei, China. He received the Ph.D. degree in electronic science and technology from Beijing Jiaotong University, Beijing, China, in 2019. From September 2017 to September 2018, he was a Visiting Student with the Department of Electrical and Computer Engineering, University of Toronto, Toronto, ON, Canada. He is currently working with the China Academy of Information and Communications Technology. His research interests include 5G wireless technology, antennas, and radio wave propagation. He received the Best Paper Award at MAPE 2015.

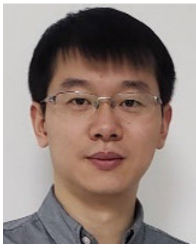

YUJIAN LI (Member, IEEE) was born in Hunan, China, in 1987. He received the B.S. and M.S. degrees in communications engineering from Beijing Jiaotong University, Beijing, China, in 2009 and 2012, respectively, and the Ph.D. degree in electronic engineering from City University of Hong Kong, in 2015.

He joined the Institute of Lightwave Technology, Beijing Jiaotong University, in 2015. He is currently a Full Professor with the School of Electronic and Information Engineering, Beijing Jiaotong University. His current research interests include millimeter-wave antennas, base station antennas, and leaky wave structures.

Dr. Li received the Outstanding Research Thesis Award from the City University of Hong Kong, in 2015, the Best Paper Award at the 2015 IEEE Asia-Pacific Conference on Antennas and Propagation (APCAP), the Best Student Paper at the 2013 National Conference on Antennas, and the Best Student Paper Award (Second Prize) at the 2013 IEEE International Workshop on Electromagnetics (iWEM). He was selected as a Finalist in the Student Paper Contest of the 2015 IEEE AP-S Symposium on Antennas and Propagation (APS). He has served as a Reviewer for the IEEE Transactions on Antennas and Propagation, the IEEE Antennas and Wireless Propagation Letters, and *IET Microwaves, Antennas & Propagation*.

BO AI (Senior Member, IEEE) received the M.S. and Ph.D. degrees from Xidian University, China, in 2002 and 2004, respectively. He is currently a Full Professor and a Ph.D. Student Advisor with the State Key Laboratory of Rail Traffic Control and Safety, Beijing Jiaotong University, China. He is also the Deputy Director of the State Key Laboratory of Rail Traffic Control and Safety. He has authored/coauthored six books and published over 230 academic research articles. He holds 21 invention patents. He is a fellow of the Institution of Engineering and Technology. He is an Editorial Committee Member of *Wireless Personal Communications*. He is also an Associate Editor of the IEEE Transactions on Consumer Electronics.